EARTH HISTORY

U-Pb geochronology of the Deccan Traps and relation to the end-Cretaceous mass extinction

Blair Schoene,[1]* Kyle M. Samperton,[1] Michael P. Eddy,[2] Gerta Keller,[1] Thierry Adatte,[3] Samuel A. Bowring,[2] Syed F. R. Khadri,[4] Brian Gertsch[3]

The Chicxulub asteroid impact (Mexico) and the eruption of the massive Deccan volcanic province (India) are two proposed causes of the end-Cretaceous mass extinction, which includes the demise of nonavian dinosaurs. Despite widespread acceptance of the impact hypothesis, the lack of a high-resolution eruption timeline for the Deccan basalts has prevented full assessment of their relationship to the mass extinction. Here we apply uranium-lead (U-Pb) zircon geochronology to Deccan rocks and show that the main phase of eruptions initiated ~250,000 years before the Cretaceous-Paleogene boundary and that >1.1 million cubic kilometers of basalt erupted in ~750,000 years. Our results are consistent with the hypothesis that the Deccan Traps contributed to the latest Cretaceous environmental change and biologic turnover that culminated in the marine and terrestrial mass extinctions.

The Deccan Traps are a continental flood basalt province that comprise >1.3 million km^3 of erupted lavas and associated rocks (*1*) that reach a total thickness of ~3000 m near the eruptive center in Western India (*2*, *3*). Paleomagnetic data (*4*–*7*) combined with K-Ar and $^{40}Ar/^{39}Ar$ geochronology of Deccan basalts (*8*, *9*) have been interpreted to indicate that >90% of the eruptive volume was emplaced rapidly (<1 million years), coincident with the Cretaceous-Paleogene boundary (KPB). This temporal relationship has long led to speculation that Deccan volcanism had a major role in the end-Cretaceous mass extinction (*10*, *11*), which saw the disappearance of nonavian dinosaurs and ammonoids, as well as major biotic turnovers in foraminifera, corals, land plants, reptiles, and mammals (*12*–*15*). However, age uncertainties from existing geochronology of the Deccan Traps (*6*, *8*, *9*) are larger than their estimated total duration, and thus the onset and duration of volcanism cannot be precisely compared to geologic, extinction, or environmental records from sedimentary sections spanning the KPB worldwide.

To better establish a high-resolution eruptive history of the main phase of Deccan volcanism, we sampled volcanic rocks from throughout the 10 formations that make up the Western Ghats (*2*, *3*, *16*) and dated them by U-Pb zircon geochronology using chemical abrasion–isotope dilution–thermal ionization mass spectrometry (CA-ID-TIMS) (*17*). Because zircon is rare in basaltic rocks, our sampling strategy targeted volcanic airfall deposits between basalt flows and high-silica and/or coarse-grained segregations within individual flows (fig. S1). The latter have been described previously in the lower half of the Deccan sequence (*18*), and we successfully extracted zircon from one such sample in the Jawhar Formation (Fm) (DEC13-30; Fig. 1). Zircon was also separated from three paleosol, or "redbole," horizons within the Ambenali and Mahabaleshwar Fms (samples RBP, RBE, and RBF; Fig. 1). These distinctive red horizons are interpreted to result from weathering of basalt during periods of volcanic quiescence (*5*). However, many also contain an evolved, high-SiO_2 volcaniclastic component (*19*), and we sampled these horizons to search for zircon-bearing volcanic ash that may have accumulated between basalt flows. Three additional zircon-bearing samples were collected from different intervals within a ~40-cm-thick green volcaniclastic bed in the Mahabaleshwar Fm. (DEC13-08, -09, and -10).

Each sample yielded a small number (typically <50) of euhedral zircon crystals with morphologies and internal zonation indicative of an igneous origin (fig. S3). Single grains were selected for analysis, photographed, pretreated, dissolved, and analyzed using CA-ID-TIMS (*17*). A subset of samples with an adequate number of grains was analyzed at both Princeton University (PU) and the Massachusetts Institute of Technology (MIT) to assess interlaboratory bias. Resulting $^{206}Pb/^{238}U$ dates from individual zircons from each sample scatter outside of analytical uncertainty (all uncertainties reported at the 2σ level; data shown in Fig. 2 and figs. S2 and S4 and reported in table S1) but show a similar spread in dates for samples analyzed at both MIT and PU. Given the excellent analytical reproducibility between laboratories (fig. S2), we discuss our results as a single data set below.

The spread in $^{206}Pb/^{238}U$ dates from our individual samples cannot be attributed to analytical uncertainties alone (fig. S2), and we interpret this dispersion to result from either prolonged growth of zircon before eruption and/or incorporation of zircon from slightly older eruptions at the same vent. This phenomenon is due to the ability of zircon to retain radiogenic Pb at magmatic temperatures (>700° to 900°C) and can result in zircon dates within volcanic deposits that predate eruption by 10^3 to 10^6 years (*20*, *21*). Given that our goal is to date the deposition of the volcanic ash, taking a weighted mean of all data from single samples is inappropriate and could bias our dates too old (*21*). Alternatively, the youngest zircon from each deposit may serve as a maximum age for deposition (*16*). However, this approach assumes that chemical abrasion has completely mitigated Pb loss (*17*) and could bias our dates too young if this assumption is not true.

To address these potential biases, we analyzed the trace element geochemistry of the dissolved zircon after routine ion exchange separation of U and Pb (*17*). By asserting that cogenetic zircons from an ashfall should have the same age and the same trace element signature, we identified the population of zircon from our data set that is amenable to statistical grouping (Fig. 2) while alleviating the concern that older, inherited zircon may bias weighted mean dates too old. We find that two or more zircons from each sample meet these criteria, and we calculate weighted means from those grains. Additionally, zircons from different samples have very different trace element signatures, supporting our interpretation that each dated horizon contains a distinct population of zircon with independent age information.

As a further means of refining our age model for the middle Ambenali–lower Mahabaleshwar Fms, we employed a Markov chain Monte Carlo analysis that imposes the law of superposition as a boundary condition (*17*). Given that stratigraphic horizons young upward, this Bayesian approach uses the $^{206}Pb/^{238}U$ dates for each horizon derived above as priors and calculates new uncertainty distributions for each sample that maximize and evaluate the probability that stratigraphically higher beds are younger. Two of three samples from the composite ashbed fail this test (DEC13-08 and -09), and thus the date arising from the third sample (DEC13-10) is used as our best estimate for the deposition of that composite ashbed. Dates derived from the redbole horizons pass the superposition test, consistent with our interpretation based on grain morphology and geochemistry that zircon from these horizons derive from primary volcanic ashfall rather than, for example, eolian transport. The depositional ages presented in Fig. 2 are those from the Monte Carlo analysis, whereas several different interpretations of the geochronological data are presented in table S3.

Regardless of the method used for U-Pb age interpretation, our main conclusions remain unaffected. The U-Pb dates reported here have corresponding uncertainties that are one to two orders of magnitude smaller than previously

[1]Department of Geosciences, Princeton University, Princeton, NJ 08540, USA. [2]Department of Earth, Atmospheric, and Planetary Sciences, Massachusetts Institute of Technology, Cambridge, MA 02139, USA. [3]Institut des Sciences de la Terre (ISTE), Université de Lausanne, GEOPOLIS, CH-1015 Lausanne, Switzerland. [4]Department of Geology, Amravati University, Amravati, India.
*Corresponding author. E-mail: bschoene@princeton.edu

published geochronology from the Deccan Traps and can thus resolve age differences between the base and top of the main eruptive phase. Using the dates from the lower- and upper-most samples (Fig. 1), we calculate a duration of 753 ± 38 thousand years (ky) for an estimated 80 to 90% of the total eruptive volume of the Deccan Traps.

These data also calibrate the timing of magnetic polarity Chron 29r, which serves as a basis for global correlation of KPB sections. The C29r/C29n reversal was previously identified within the lower Mahabaleshwar Fm (*5*), from which we collected samples RBP, RBE, and RBF. We use the $^{206}Pb/^{238}U$ date of sample RBE of 65.552 ± 0.026/0.049/0.086 million years ago (Ma) (2σ uncertainties given here as internal only/with tracer calibration/with ^{238}U decay constant) as our best estimate for the age of C29r/C29n reversal because it was sampled from between two basalts with transitional polarity (Fig. 1) (*5*). The basal age of C29r is constrained by sample DEC13-30, which was collected from a basaltic segregation vein within the Jawhar Fm near the base of the main Deccan phase and yielded a $^{206}Pb/^{238}U$ date of 66.288 ± 0.027/0.047/0.085 Ma. From the same outcrop, Chenet *et al.* (*9*) reported transitional magnetic polarity just tens of meters beneath lavas containing reverse polarity (C29r); from this transitional horizon they reported a K-Ar date of 67.4 ± 2.0 Ma. Though their date was interpreted to represent the C30r/C30n or C31n/C30r transition, with a long hiatus in eruptions represented in that section (*9*), our U-Pb date from DEC13-30 is not consistent with a hiatus of that magnitude. A simpler interpretation is that the transitional polarity basalts represent the C30n/C29r transition. Thus, the age difference between DEC13-30 and RBE of 736 ± 37 ky is also the length of C29r. An independent estimate for the length of C29r from cyclostratigraphic analysis of marine Ocean Drilling Program (ODP) cores and the Zumaia section, Spain, yields durations of 713 to 725 ky (*22*), in good agreement with our calibration based on U-Pb geochronology.

Our results also have implications for the age of the KPB and associated mass extinction event, as several estimates for the duration of the Cretaceous portion of C29r of 300 to 340 ky have recently been published based on cyclostratigraphy of magnetically and biostratigraphically calibrated ODP sections (*23*). Using our date for the C30n/C29r reversal and the average cyclostratigraphic estimate yields an age for the KPB of 65.968 ± 0.085 Ma (including systematic uncertainties), which agrees well with a recently reported KPB age of 66.043 ± 0.086 Ma (also including full systematic uncertainties) from $^{40}Ar/^{39}Ar$ geochronology on tephras that bracket the terrestrial KPB near Hells Creek, Montana (*24*). Determining an age for the KPB by back-calculation from our estimate for the C29r/C29n reversal is more problematic in that estimates for the Paleogene portion of C29r based on cyclostratigraphy of the Zumaia KPB section range from 206 to 398 ky (*22*, *25*). Regardless, the combination of our geochronologic data with cyclostratigraphic estimates effectively rules out any age for the KPB younger than 65.740 ± 0.086 Ma.

Although the temporal relationship between large igneous provinces and mass extinctions is well established (*26*), the potential kill mechanisms remain a subject of debate. Models of proposed drivers focus on volcanically sourced CO_2, SO_2, and halogens, which can cause global warming and/or cooling on different time scales (*27*); acid

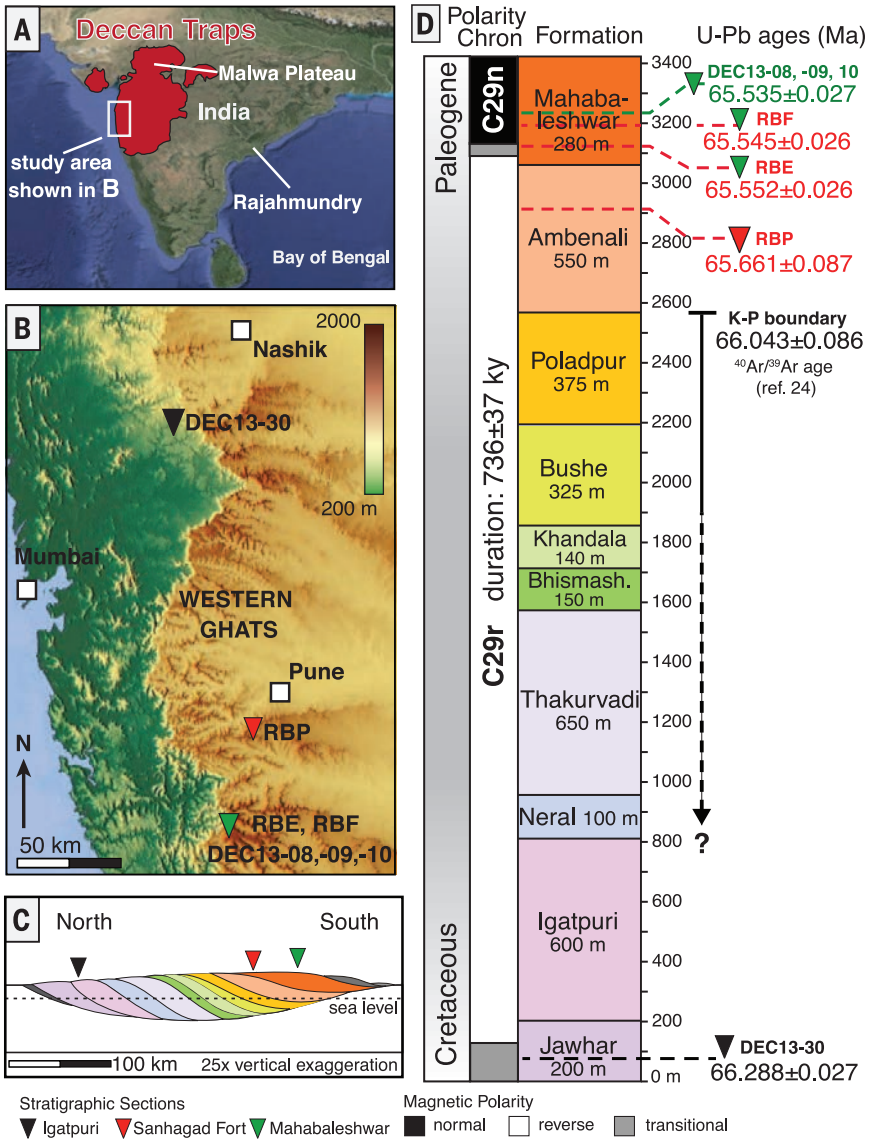

Fig. 1. Geography and stratigraphy of the Deccan Traps. (**A**) Aerial extent of the Deccan Traps colored in red. (**B**) Shaded relief map of study area in the Western Ghats. Major cities are indicated by white squares. Approximate locations of sampling transects and samples are indicated by colored triangles; transects are named at the bottom of the figure. The color bar (top right) shows elevation in meters, highlighting the escarpment where the best exposures of Deccan lavas occur. (**C**) Schematic cross section of Deccan lavas, from Chenet *et al.* (*4*), showing general southerly dip and younging to the south. Sampling transects are indicated by colored triangles. Colors correspond to the formations named in (D). (**D**) Composite stratigraphic section of the Deccan Traps in the Western Ghats, with approximate formation thicknesses shown. The geologic time scale is on the left, with the gray area corresponding to the unknown location of the KPB within the Deccan Traps. The geomagnetic polarity time scale is shown, with relevant chrons labeled and polarity indicated by black, white, or gray. The duration of C29r is the difference between the ages of DEC13-30 and RBE. U-Pb ages are shown on the right and are color-coded for sample type: black, segregation vein in basalt; red, volcanic material from paleosol; green, volcanic ashbed. Colored triangles correspond to sampling transects shown in (B) and (C). The date for KPB from Renne *et al.* (*24*) includes full systematic uncertainties. U-Pb age uncertainties are 2σ and include internal uncertainties only; ages with full systematic uncertainties are ~±0.085 Ma. See text and table S3 for full uncertainty budget and Fig. 2 and table S1 for data.

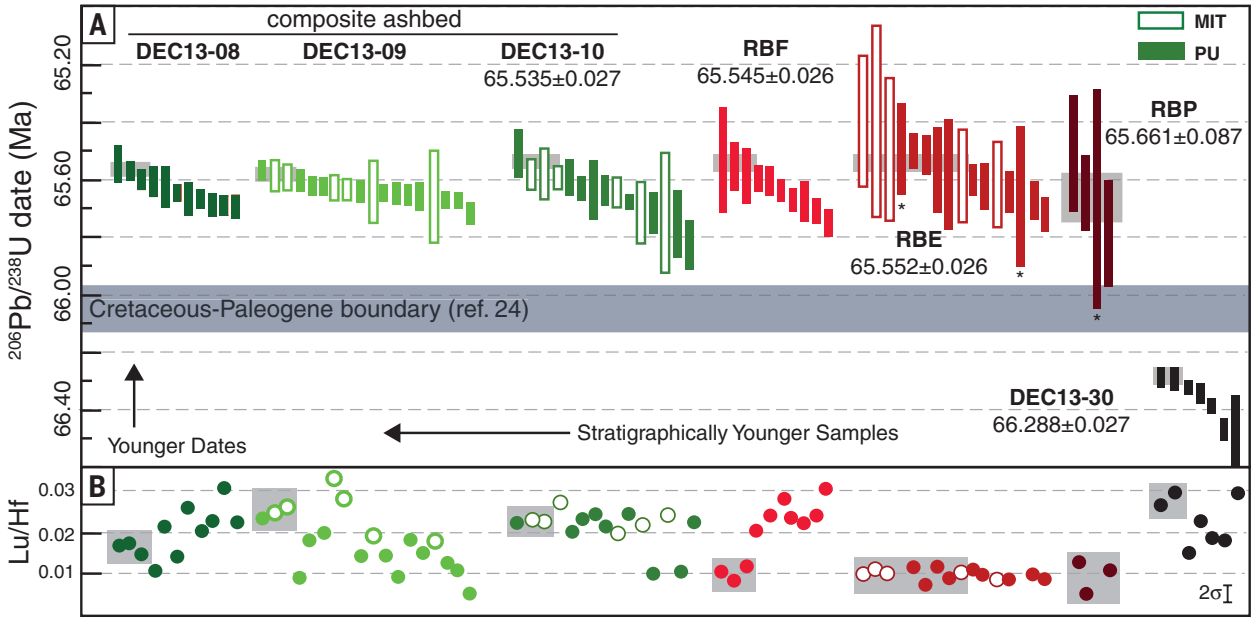

Fig. 2. U-Pb zircon CA-ID-TIMS geochronological data. (**A**) Rank order plot of U-Pb data presented in this study, color-coded by sample type in Fig. 1 and with sample name next to data. Sample locations are shown in Fig. 1. The vertical axis indicates $^{206}Pb/^{238}U$ date, and rectangle height corresponds to 2σ uncertainties for single-crystal zircon analyses, with internal uncertainties only. MIT and PU indicate the laboratory used. Stratigraphic younging is shown from right to left. The horizontal gray band shows the date for KPB from Renne *et al*. (*24*). Small gray rectangles behind the data indicate the youngest zircons that were indicated to be cogenetic by comparing dates and geochemistry in (B), from which weighted means were calculated. Dates indicated beneath sample names result from the Monte Carlo Markov chain simulation that uses weighted mean dates and imposes the law of superposition to arrive at our best estimates for the time of deposition of the dated horizons (*17*). Asterisks indicate zircon without trace element geochemistry. U-Pb data are given in table S1. (**B**) Lutetium/hafnium (Lu/Hf) ratios of the same volume of dated zircon, younging from right to left as in (A). Gray boxes indicate zircons determined to be cogenetic due to same age and geochemistry. The full geochemical data set is presented in table S2 and plotted in fig. S5.

rain and ozone reduction (*28*); and ocean acidification (*29*). Late Cretaceous records beginning near the C30n/C29r transition, and therefore near the onset of the main phase of Deccan volcanism, show a decrease in $\delta^{18}O$ values of foraminifera (*30*) and morphological changes in fossil leaves (*31*) that are consistent with instabilities in global temperature. A two-stage decline in seawater $^{187}Os/^{188}Os$ values initiating at the C30n/C29r reversal was interpreted to record weathering of the Deccan Traps, predating a second decline in $^{187}Os/^{188}Os$ and a synchronous Ir spike that were attributed to the Chicxulub impact (*32*). Furthermore, biostratigraphic records show increased rates of biotic turnover in mammals, amphibians, land plants, and foraminifera through the Cretaceous portion of C29r preceding the peak extinction interval (*12*, *13*, *15*, *31*, *33*). Additional testing of the influence of the Deccan Traps on these records will require further determination of eruption tempos and hiatuses coupled with realistic estimates of volatile release from individual eruptive phases (*34*) that can be temporally linked to paleoenvironmental proxies. Our results are a critical part of this discussion as they are consistent with the hypothesis that environmental and ecological deterioration began with eruption of the Deccan Traps before the Chicxulub impact and the end-Cretaceous mass extinction. Therefore, both the Chicxulub impact and eruption of the Deccan Traps should be considered in any model for the extinction.

REFERENCES AND NOTES

1. A. E. Jay, M. Widdowson, *J. Geol. Soc. London* **165**, 177–188 (2008).
2. S. Khadri, K. Subbarao, P. Hooper, J. Walsh, *Geol. Soc. India Mem.* **10**, 281 (1988).
3. J. E. Beane, C. A. Turner, P. R. Hooper, K. V. Subbarao, J. N. Walsh, *Bull. Volcanol.* **48**, 61–83 (1986).
4. A.-L. Chenet *et al*., *J. Geophys. Res.* **114**, B06103 (2009).
5. A.-L. Chenet, F. Fluteau, V. Courtillot, M. Gérard, K. V. Subbarao, *J. Geophys. Res.* **113**, B04101 (2008).
6. V. Courtillot *et al*., *Earth Planet. Sci. Lett.* **182**, 137–156 (2000).
7. D. Vandamme, V. Courtillot, *Phys. Earth Planet. Inter.* **74**, 241–261 (1992).
8. C. Hofmann, G. Féraud, V. Courtillot, *Earth Planet. Sci. Lett.* **180**, 13–27 (2000).
9. A. Chenet, X. Quidelleur, F. Fluteau, V. Courtillot, S. Bajpai, *Earth Planet. Sci. Lett.* **263**, 1–15 (2007).
10. V. Courtillot *et al*., *Earth Planet. Sci. Lett.* **80**, 361–374 (1986).
11. G. Keller *et al*., *Earth Planet. Sci. Lett.* **341–344**, 211–221 (2012).
12. G. P. Wilson, *Geol. Soc. Am. Spec. Pap.* **503**, 365 (2014).
13. N. Macleod *et al*., *J. Geol. Soc. London* **154**, 265–292 (1997).
14. P. Schulte *et al*., *Science* **327**, 1214–1218 (2010).
15. J. Punekar, P. Mateo, G. Keller, *Geol. Soc. Am. Spec. Pap.* **505**, 91 (2014).
16. K. G. Cox, C. J. Hawkesworth, *J. Petrol.* **26**, 355–377 (1985).
17. Materials and methods are available on *Science* Online.
18. N. R. Bondre, R. A. Duraiswami, G. Dole, *Bull. Volcanol.* **66**, 29–45 (2004).
19. M. Widdowson, J. N. Walsh, K. V. Subbarao, *Geol. Soc. London Spec. Publ.* **120**, 269–281 (1997).
20. J. I. Simon, P. R. Renne, R. Mundil, *Earth Planet. Sci. Lett.* **266**, 182–194 (2008).
21. B. Schoene, J. Guex, A. Bartolini, U. Schaltegger, T. J. Blackburn, *Geology* **38**, 387–390 (2010).
22. T. Westerhold *et al*., *Palaeogeogr. Palaeoclimatol. Palaeoecol.* **257**, 377–403 (2008).
23. S. J. Batenburg *et al*., *J. Geol. Soc. London* **171**, 165–180 (2014).
24. P. R. Renne *et al*., *Science* **339**, 684–687 (2013).
25. F. J. Hilgen, K. F. Kuiper, L. J. Lourens, *Earth Planet. Sci. Lett.* **300**, 139–151 (2010).
26. V. E. Courtillot, P. R. Renne, *C. R. Geosci.* **335**, 113–140 (2003).
27. M. Mussard, G. Le Hir, F. Fluteau, V. Lefebvre, Y. Goddéris, *Geol. Soc. Am. Spec. Pap.* **505**, 339 (2014).
28. B. A. Black, J.-F. Lamarque, C. A. Shields, L. T. Elkins-Tanton, J. T. Kiehl, *Geology* **42**, 67–70 (2014).
29. R. A. Feely *et al*., *Science* **305**, 362–366 (2004).
30. L. Li, G. Keller, *Geology* **26**, 995–998 (1998).
31. P. Wilf, K. R. Johnson, B. T. Huber, *Proc. Natl. Acad. Sci. U.S.A.* **100**, 599–604 (2003).
32. N. Robinson, G. Ravizza, R. Coccioni, B. Peucker-Ehrenbrink, R. Norris, *Earth Planet. Sci. Lett.* **281**, 159–168 (2009).
33. G. P. Wilson, D. G. DeMar, G. Carter, *Geol. Soc. Am. Spec. Pap.* **503**, 271 (2014).
34. S. Self, S. Blake, K. Sharma, M. Widdowson, S. Sephton, *Science* **319**, 1654–1657 (2008).

ACKNOWLEDGMENTS

This work was supported by the Department of Geosciences Scott Fund at Princeton University and the U.S. NSF through the Continental Dynamics Program, Sedimentary Geology and Paleobiology Program, and the Office of International Science and Engineering's India Program under grants EAR-0447171 and EAR-1026271 to G.K. P. Kemeny assisted with fieldwork and sample collection; A. Chen assisted with sample processing. MIT's analytical work was supported by the Robert Shrock chair. All data associated with this work can be found in the supplementary materials (*17*).

SUPPLEMENTARY MATERIALS

www.sciencemag.org/content/347/6218/182/suppl/DC1
Materials and Methods
Figs. S1 to S5
Tables S1 to S3
References (*35–108*)

9 October 2014; accepted 26 November 2014
Published online 11 December 2014;
10.1126/science.aaa0118